



Rapid Warming of Sea Surface Temperature along the Kuroshio and the China Coast in the East China Sea during the Twentieth Century

YOSHI N. SASAKI^a AND CHISATO UMEDA^a

^a Faculty of Science, Hokkaido University, Sapporo, Japan

(Manuscript received 4 June 2020, in final form 8 March 2021)

ABSTRACT: It has been reported that the sea surface temperature (SST) trend of the East China Sea during the twentieth century was a couple of times larger than the global mean SST trend. However, the detailed spatial structure of the SST trend in the East China Sea and its mechanism have not been understood. The present study examines the SST trend in the East China Sea from 1901 to 2010 using observational data and a Regional Ocean Modeling System (ROMS) with an eddy-resolving horizontal resolution. A comparison among two observational datasets and the model output reveals that enhanced SST warming occurred along the Kuroshio and along the coast of China over the continental shelf. In both regions, the SST trends were the largest in winter. The heat budget analysis using the model output indicates that the upper-layer temperature rises in both regions were induced by the trend of ocean advection, which was balanced in relation to the increase of surface net heat release. In addition, the rapid SST warming along the Kuroshio was induced by the acceleration of the Kuroshio. Sensitivity experiments revealed that this acceleration was likely caused by the negative wind stress curl anomalies over the North Pacific. In contrast, the enhanced SST warming along the China coast resulted from the ocean circulation change over the continental shelf by local atmospheric forcing.


KEYWORDS: Boundary currents; Atmosphere-ocean interaction; Climate change; Ocean models; Oceanic variability; Trends

1. Introduction

The rising of sea temperature has attracted considerable attention because of its relation to global warming (e.g., Trenberth et al. 2007; Rhein et al. 2013). For example, the linear trend of the global mean temperature in the upper 75 m depth from 1971 to 2010 is $+0.11^{\circ}\text{C decade}^{-1}$ (Levitus et al. 2009; Rhein et al. 2013). Sea surface temperature (SST) is one of the key variables in understanding the warming, as the surface ocean directly responds to atmospheric warming. In addition, long-term observational data are available on SST. Importantly, SST warming is not spatially uniform. For example, previous studies have identified particularly fast warming along western boundary currents (e.g., Wu et al. 2012; Yang et al. 2016). Clarifying the mechanisms of this fast warming is important for understanding climate change (e.g., Small et al. 2008; Kelly et al. 2010). In the present study, we focus the SST warming in the East China Sea (Fig. 1), a marginal sea east of China and west of Japan. In the East China Sea, the Kuroshio, which is the western boundary current of the subtropical gyre in the North Pacific, flows northward along the continental slope (Fig. 1; Kida et al. 2015). SST variability in the East China Sea has a substantial influence on the atmosphere (e.g., Xie et al. 2002; Xu et al. 2011; Sasaki et al. 2012; Miyama et al. 2012).

Many studies have reported the SST trend of the East China Sea (e.g., Belkin 2009; Tang et al. 2009; Wu et al. 2012; Bao and Ren 2014). Nevertheless, studies examining the mechanism of the SST rise in the East China Sea are limited. Zhang et al. (2010) performed a heat budget analysis using a reanalysis product from 1958 to 2010 and demonstrated qualitatively that the warming around the Kuroshio corresponded to an increase in the anomalous ocean advection and damping by surface heat flux. Cai et al. (2017) also demonstrated the importance of ocean advection on the SST warming of the East China Sea using a reanalysis product from 1958 to 2014. On the other hand, Yeh and Kim (2010) investigated the wintertime SST trend of the East China Sea from 1950 to 2008 using observational and reanalysis datasets and revealed that the SST rise was caused by surface latent and sensible heat flux forcings associated with the North Pacific oscillation-like sea level pressure changes. It needs to be considered that the study periods of these previous studies have not included the entire twentieth century. For a better understanding of the warming trend, a longer data analysis is necessary. In addition, the horizontal resolutions of observational and reanalysis data have generally been too low ($\sim 0.5^{\circ}$) to clarify the spatial structure of the SST trend in the East China Sea. Further, the heat budget of the reanalysis products has generally not been closed. All this considered, the purpose of the present study is to clarify the mechanism of the SST trend in the East China Sea during the twentieth century using the output of a regional ocean model as well as observational datasets.

The rest of the paper is organized as follows. In section 2, we describe the datasets, regional ocean model settings, and the methods used in studying the mechanism of the SST trend in

 Denotes content that is immediately available upon publication as open access.

Corresponding author: Yoshi N. Sasaki, sasakiyo@sci.hokudai.ac.jp

DOI: 10.1175/JCLI-D-20-0421.1

© 2021 American Meteorological Society. For information regarding reuse of this content and general copyright information, consult the AMS Copyright Policy (www.ametsoc.org/PUBSReuseLicenses).

Brought to you by SEOUL NATL UNIV. LIBRARY | Unauthenticated | Downloaded 09/23/22 01:58 AM UTC

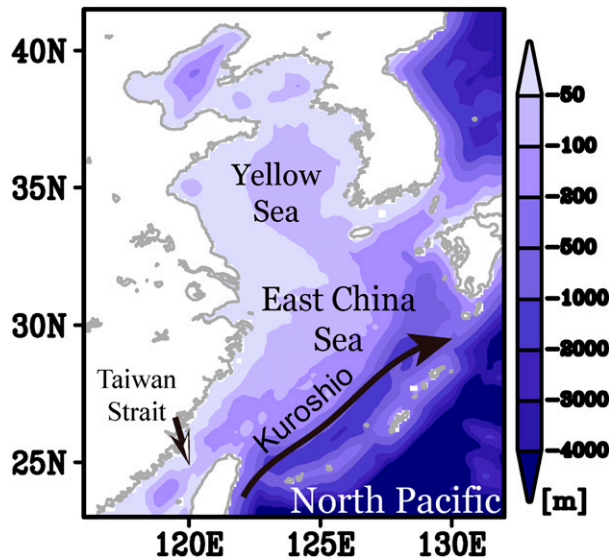


FIG. 1. Bottom topography of the model with a schematic of the Kuroshio in the East China Sea.

the East China Sea. Then, the detailed spatial structure of the SST trend and its mechanism are examined in section 3. Finally, a summary and discussion are presented in section 4.

2. Data and methods

a. Model

We used the Regional Ocean Modeling System (ROMS), which solves free-surface primitive equations using the hydrostatic and Boussinesq approximations on a generalized terrain-following sigma vertical coordinate system (Haidvogel et al. 2000; Shchepetkin and McWilliams 2005). The model domain covered an area from 23° to 41.5°N and from 116° to 132°E with a horizontal resolution of $0.1^\circ \times 0.1^\circ$ and a vertical resolution of 32 sigma levels (Fig. 1). The choice of the horizontal resolution was based on previous studies suggesting the importance of having a high horizontal resolution of less than 10 km in reproducing the flow field of the East China Sea (Guo et al. 2003; Yang et al. 2011) and mesoscale features (e.g., Na et al. 2014). The minimum depth within the model domain was 20 m.

The model was run from 1871 to 2010 starting from a state of rest and using the climatological temperature and salinity fields of the *World Ocean Atlas 2009* (Antonov et al. 2010; Locarnini et al. 2010). To check the influence of the initial conditions, we performed an additional run from 1871 to 2010, in which the mean temperature and salinity from 1871 to 2010 of the former run were used as the initial conditions. Because the results of this latter run were nearly identical to those of the former run, we only present the results of the former run in this study. The surface heat flux and wind stress were calculated using the bulk formula given by Fairall et al. (1996). The calculations were performed using the daily atmospheric variables given by the National Oceanic and Atmospheric Administration Twentieth Century Reanalysis (20CR; Compo et al. 2011) from 1871 to 2010 along with the simulated SST and surface ocean current.

Lateral temperature, salinity, velocity, and surface salinity were restored to the monthly values of the Simple Ocean Data Assimilation v2.2.4 (SODA) reanalysis product from 1871 to 2010 (Giese and Ray 2011). Because the tide is important for reproducing circulation over the continental shelf (e.g., Lin et al. 2020), we used the tidal solution simulated by Oregon State University (Egbert and Erofeeva 2002) as tidal forcing along the lateral boundaries. The Changjiang River discharge was based on the monthly climatology estimated by Dai and Trenberth (2002). Following Kako et al. (2016), we added this river discharge into the uppermost layer as a point source, where the temperature was determined by monthly mean 2-m air temperature of the 20CR data from 1871 to 2010 and the salinity set 0 PSU. Hereafter, we refer to this control run as the CTL run. To exclude the spinup period, we analyzed the hindcast output from 1901 to 2010.

To elucidate the mechanism of the SST trend in the East China Sea, we performed two sensitivity experiments in addition to the CTL run. In one of these additional runs, the temperature, salinity, and velocity along the lateral boundaries were restored to the monthly climatologies from 1871 to 2010, while the other model settings were the same as those of the CTL run. Thus, the long-term trend of the model was caused by the surface momentum, and heat and freshwater fluxes. Because this run excluded influences from outside the model domain, we refer to it as the LOCAL run. The other run was the REMOTE run. In this run, the atmospheric variables used to calculate the surface momentum and heat fluxes and the downward shortwave and longwave radiations were changed to the daily climatologies from 1871 to 2010. The surface salinity for restoration and the temperature of the Changjiang River discharge were also changed to the monthly climatology from 1871 to 2010. The forcing from the lateral boundary mainly induced the long-term trend of the REMOTE run.

b. Observational datasets

To obtain the SST trend of the East China Sea during the twentieth century, we used two monthly SST datasets as well as the regional ocean model. One was provided by the UK Met Office as the Hadley Centre Sea Ice and Sea Surface Temperature dataset version 1 (HadISST; Rayner et al. 2003). This dataset was presented on a $1^\circ \times 1^\circ$ horizontal grid for the years between 1870 and 2010. The other dataset was a SST dataset presented by Minobe and Maeda (2005) and contained anomalous climatology data from the climatology for the period from 1950 to 2000. It had a horizontal resolution of $1^\circ \times 1^\circ$ and encompassed the years from 1850 to 2002. This dataset is referred to as the Minobe/Maeda dataset. The main difference between these two SST datasets is that the Minobe/Maeda dataset did not employ either spatial interpolation or smoothing for missing data areas. Thus, the Minobe/Maeda dataset contained missing values for grid areas with no observations.

In addition to these datasets, we used the version 2 of the optimum interpolation SST product (OISST; Reynolds et al. 2007) provided by the National Oceanic and Atmospheric Administration for the period from 1982 to 2010. This OISST dataset had a $0.25^\circ \times 0.25^\circ$ grid and used in situ and the Advanced Very High Resolution Radiometer SST data. Since this dataset had a high horizontal resolution, it was useful in

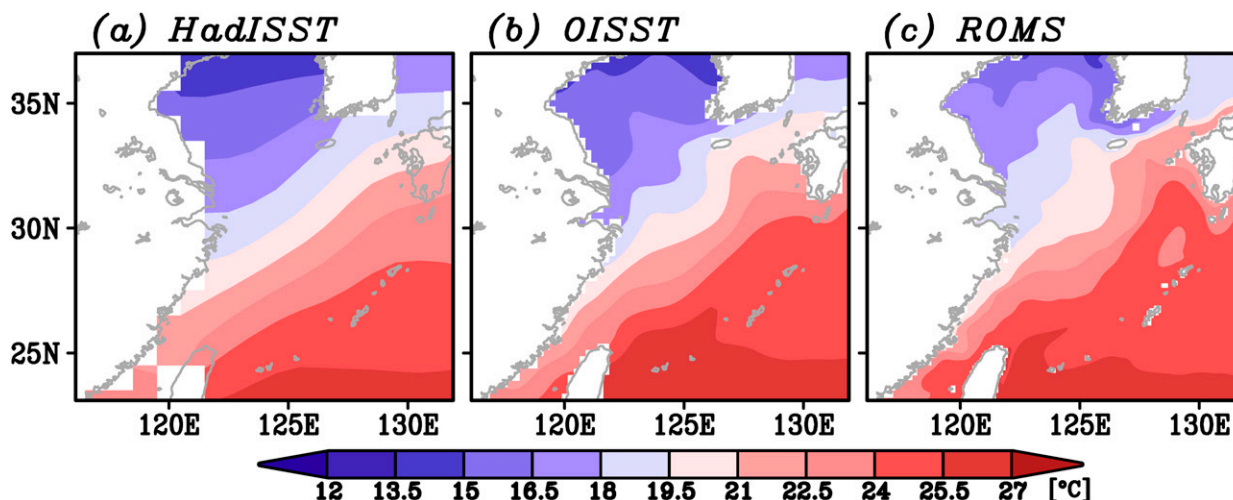


FIG. 2. Climatology of SST from (a) the HadISST dataset, (b) the OISST dataset, and (c) the CTL run. The HadISST dataset and CTL run cover the period from 1901 to 2010, while the OISST dataset covers the period from 1982 to 2010.

validating the mean SST pattern of the model simulation of the East China Sea.

c. Methods

We estimated the trend as a simple linear trend after removing the monthly climatology from 1901 to 2010. If the missing data for a grid area of the Minobe/Maeda dataset were greater than 40% during the study period, the trend of that grid area was set as missing in time. The statistical significance of the linear trend was assessed using a Student's t test, for which the effective degree of freedom of the time series was estimated using the method presented by [Santer et al. \(2000\)](#) to consider the effect of low-frequency variability. To estimate the statistical significance of the correlation coefficients, we used a Monte Carlo method. According to this method, 1000 random time series were created via a phase randomization technique to produce surrogate time series that had similar temporal variability spectra to that of the original time series ([Kaplan and Glass 1995](#)). In the present study, a 95% confidence level was used for both the trend and correlation analyses.

3. Results

a. Spatial structure of the sea surface temperature trend

Before investigating the SST trend of the East China Sea, we compared the long-term mean SST pattern among the HadISST and OISST datasets and the CTL simulation ([Fig. 2](#)). It was found that the CTL run was able to successfully reproduce the basic features of the observational datasets on the climatological SST in the East China Sea. These indicated that the SST was warm in the southeast, with the temperature decreasing toward the northwest. Both the OISST dataset and the model revealed that the SST had a warm tongue structure along the Kuroshio axis at 26°N, 126°E, although the HadISST dataset did not, probably due to its low horizontal resolution. The model showed a warm SST bias along the western coast of Japan at 32°N, 129°E due to the northward overshooting of the Kuroshio.

[Figure 3](#) shows the linear SST trends of the two observational datasets (HadISST and Minobe/Maeda) and the CTL run from 1901 to 2010. First, we compared the trends between the two observational datasets ([Figs. 3a,b](#)). Although the SST trend was positive and was statistically significant for almost the entire East China Sea, there did exist two broad peaks. One was located over the continental shelf along the China coast over the continental shelf extending to the Taiwan Strait, and the other along the Kuroshio. The amplitude of the SST trends obtained from the HadISST dataset tended to be larger than those obtained from the Minobe/Maeda dataset. These enhanced SST warmings along the coast of China and the Kuroshio were successfully simulated by the CTL run ([Fig. 3c](#)). The amplitude of the simulated SST trend was generally between those of the two observational datasets. Hence, it can be concluded that the CTL run successfully reproduced the SST trend in the East China Sea. A two-peak structure in the SST trend of the East China Sea has not been previously reported. Note that the SST trend of the SODA re-analysis product does not show this two-peak structure (not shown).

To examine the temporal structure of the SST trend in detail, the SST anomalies were regionally averaged along the China coast and the Kuroshio ([Fig. 4](#)). Every SST time series of the three datasets averaged along the Kuroshio exhibited continuous SST warming ([Fig. 4a](#)). The SST warming per 100 years along the Kuroshio of the HadISST dataset, the Minobe/Maeda dataset, and the CTL run were $+1.68^{\circ}$, $+1.15^{\circ}$, and $+1.72^{\circ}\text{C}$, respectively. These results are consistent with the aforementioned conclusion that our model successfully simulated the SST warming in this region. Note that these SST trends in the East China Sea were larger than the global mean SST trend ($+0.62^{\circ} \pm 0.14^{\circ}\text{C}$ from 1900 to 2008; [Wu et al. 2012](#)). Similarly, the model successfully reproduced the continuous warming along the China coast over the continental shelf ([Fig. 4b](#)). The linear SST trends of the HadISST dataset, the Minobe/Maeda dataset, and the CTL run along the China coast were $+2.11^{\circ}$, $+1.23^{\circ}$, and $+1.63^{\circ}\text{C}$ (100 yr^{-1}), respectively. The unrealistic peak of the Minobe/Maeda dataset in 1944 was probably due to

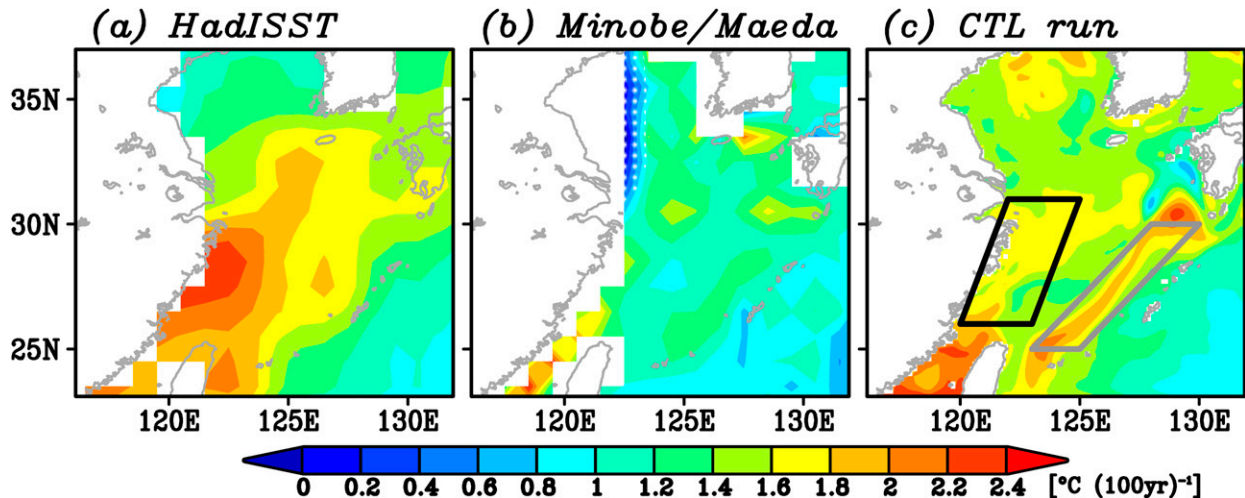


FIG. 3. Linear trend of SST from (a) the HadISST dataset, (b) the Minobe/Maeda dataset, and (c) the CTL run. The HadISST dataset and the CTL run cover the period from 1901 to 2010, while the Minobe/Maeda dataset covers the period from 1901 to 2002. The parallelograms over the continental shelf (black) and along the Kuroshio (gray) in (c) denote the regions in which the area-averaged SSTs were calculated in Fig. 4. The regions in which the trend is not statistically significant at a 95% confidence level are stippled.

the shortage of data during the 1940s. In both regions, the acceleration of the SST rises around the 1980s reported by Zhang et al. (2010) and Yeh and Kim (2010) was not observed. The ability of the model to simulate the interannual and interdecadal SST variability is worth noting. The detrended SST time series averaged along the Kuroshio of the CTL run was significantly correlated with that of both the HadISST ($r = 0.50$) and Minobe/Maeda ($r = 0.53$) datasets. The detrended SST time series averaged along the China coast was also significantly correlated with that of both the HadISST ($r = 0.68$) and Minobe/Maeda ($r = 0.50$) datasets. These results indicate that our simulation was able to reproduce interannual to interdecadal SST variability in the East China Sea as well as the SST trend.

We next performed an empirical orthogonal function (EOF) analysis to examine the SST variability of the East China Sea during the study period. The first EOF mode of the annual mean SST of the CTL run accounted for 80.8% of total SST variance in the East China Sea from 1901 to 2010. The spatial pattern of this mode included the two peaks along the Kuroshio and the China coast over the continental shelf (not shown), which was consistent with the SST trend shown in Fig. 3. The corresponding principal component of the first EOF mode exhibited a prominent trend (not shown), and its detrended time series was highly correlated with the time series for the detrended SST averaged over the Kuroshio ($r = 0.81$) and over the China coast ($r = 0.88$). Thus, the SST trend of the East China Sea shown in Fig. 3 represents the dominant mode of SST variability in the East China Sea from 1901 to 2010.

The SST trend along the Kuroshio was associated with a peak in the subsurface (Fig. 5). The peak around the Kuroshio had an amplitude of $+2.8^{\circ}\text{C} (100\text{ yr})^{-1}$ for a depth of approximately 80 m. Below this maximum, the amplitude of the temperature trend decreased with depth, becoming zero around 500 m. A similar subsurface maximum in the temperature trend can be observed in other latitude bands (not shown). On the other

hand, the SST trend along the China coast did not extend to the bottom of the continental shelf. Because the subsurface maximum of the trend implies the damping of the temperature trend by surface forcings, the feature along the Kuroshio indicates the

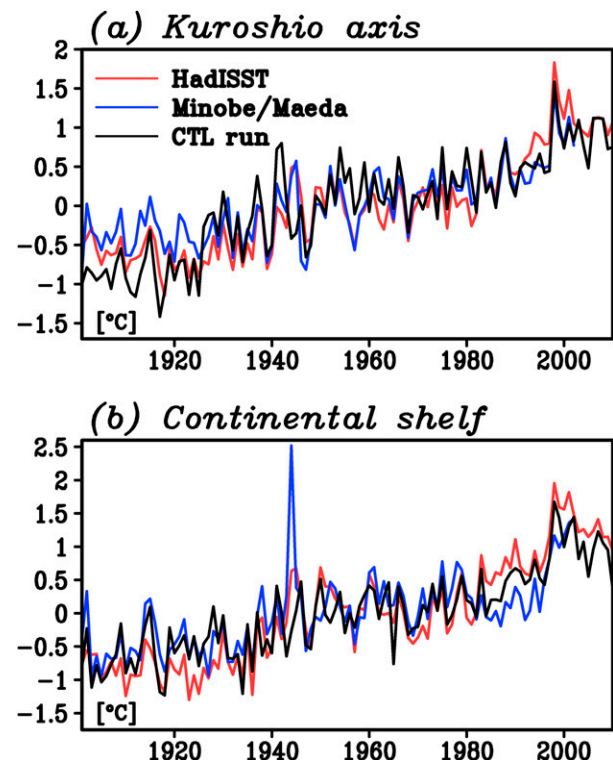


FIG. 4. The annual mean SST anomalies of the three datasets [see legend in (a)] averaged (a) along the Kuroshio and (b) over the continental shelf. These are shown as gray and black parallelograms in Fig. 3c, respectively.

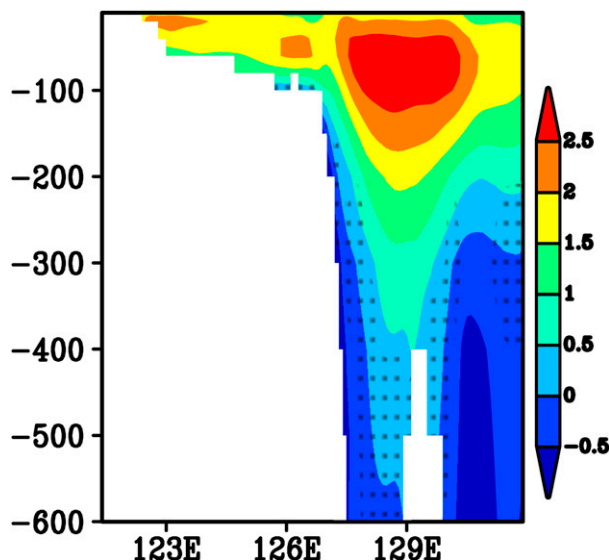


FIG. 5. Vertical section of the temperature trend along 29°N from 1901 to 2010 obtained from the CTL run. The units are $^{\circ}\text{C} (100 \text{ yr})^{-1}$. The regions in which the trend is not statistically significant at a 95% confidence level are stippled.

importance of oceanic heat advection to the warming trend. This point will be demonstrated in the next subsection.

The SST trends along the Kuroshio and the coast of China showed significant seasonal dependency. The SST trend of the CTL run showed that the trend was the largest in the winter (Fig. 6). This seasonal dependency is consistent with that found in the HadISST and Minobe/Maeda datasets (not shown) and in previous studies (e.g., Zhang et al. 2010), although the wintertime SST trend along the Kuroshio was overestimated by the CTL run. The SST trend of the continental shelf in autumn was larger than that in spring.

In contrast, the seasonal march of the vertical temperature shows a different seasonal dependency (Fig. 7). In winter, the temperature trends both along the China coast over the continental shelf and along the Kuroshio were vertically uniform. However, the subsurface temperature trend was larger than the SST trend in summer along the Kuroshio. This vertical structure of the temperature trend in summer is consistent with the aforementioned idea that the subsurface maximum of the temperature trend was due to the damping by surface forcings.

It is informative to compare the SST trend of the East China Sea to the trend of the atmospheric temperature over the sea. The 2-m atmospheric temperature also had a warming trend, but its spatial pattern was different from that of the SST trend (Fig. 8b). The surface atmospheric temperature trend had a monopole structure over the East China Sea with a peak around Taiwan. This monopole structure was associated with the southerly wind trend (i.e., the weakening of the climatological northerly wind) (Fig. 8a). This difference in the spatial structures between the atmospheric temperature and the SST trends could be partly due to the low spatial resolution of the atmospheric reanalysis dataset, but it nonetheless indicates the importance of the oceanic role in SST warming.

b. Heat budget analysis for the sea surface temperature trend

In the previous subsection, it was found using two observational datasets and the CTL run that rapid SST warming occurred in the East China Sea along the Kuroshio and the China coast over the continental shelf from 1901 to 2010 (Fig. 3). However, the spatial patterns of the SST trend were different from those of the surface atmospheric temperature trend (Fig. 8b). To clarify the mechanism of the SST trend, we conducted a heat budget analysis using the output of the CTL run.

The heat equation consisted of four terms: temperature tendency ($\partial T / \partial t$), advection ($\mathbf{v} \cdot \nabla T$), net surface heat flux, and diffusion, where T is temperature and \mathbf{v} is the velocity vector. Each term was calculated online using the model (Wilkin 2006). The net surface heat flux is the sum of the latent and sensible heat flux and the shortwave and longwave radiation (upward positive). We estimated the 0–100-m-depth averages of each term and calculated their linear trends. Note that the spatial pattern of the temperature trend averaged over 0–100 m depth was similar to that of the SST trend (not shown). Because the temperature tendency term is generally small on decadal and longer time scales (e.g., Xie et al. 2010; Sasaki and Schneider 2011), we investigated the trends of the other three terms of the heat equation and their balance.

Figure 9 shows the linear trend of each of the three terms of the heat equation. The trend of the advection term had positive values both along the China coast over the continental shelf and along the Kuroshio (Fig. 9c), where SST warming was prominent. The amplitude of the trend of the advection term averaged along the China coast over the continental shelf and along the Kuroshio was approximately $+1.3^{\circ}$ and $+0.4^{\circ}\text{C yr}^{-1} (100 \text{ yr})^{-1}$, respectively. These values mean that the advection term acted to increase the water temperature by approximately $+0.5$ – 1.5°C during each year at the end of the twentieth century compared to the first years of the twentieth century. The positive trends in these regions were large enough to explain the SST trends (Fig. 3), indicating that increasing temperature advection induced the upper-layer temperature rise in both regions. In contrast, the trend of the net surface heat flux was negative in these regions (Fig. 9a), while the trend of the diffusion term was small and can be ignored (Fig. 9b). Thus, the trend of the net surface heat flux was roughly balanced in relation to the trend of heat advection in many regions, damping the upper-layer temperature trend. These results are consistent with those of Zhang et al. (2010), although their study period is after 1958. For the net surface heat flux trend, the latent heat flux trend was the dominant contributor compared with the sensible heat flux and the radiation flux along the Kuroshio (not shown). The subsurface maximum in the temperature trend (Fig. 5) can also be explained by these results: the damping by the net surface heat flux reduced the amplitude of the surface warming induced by oceanic heat advection. Note that this subsurface maximum of the temperature trend did not correspond to the maximum vertical gradient of mean temperature, implying that the vertical thermocline shift was not important for the subsurface maximum of the temperature trend.

The trends of the three terms of the heat equation in each season also showed the seasonal dependency. The trend of the

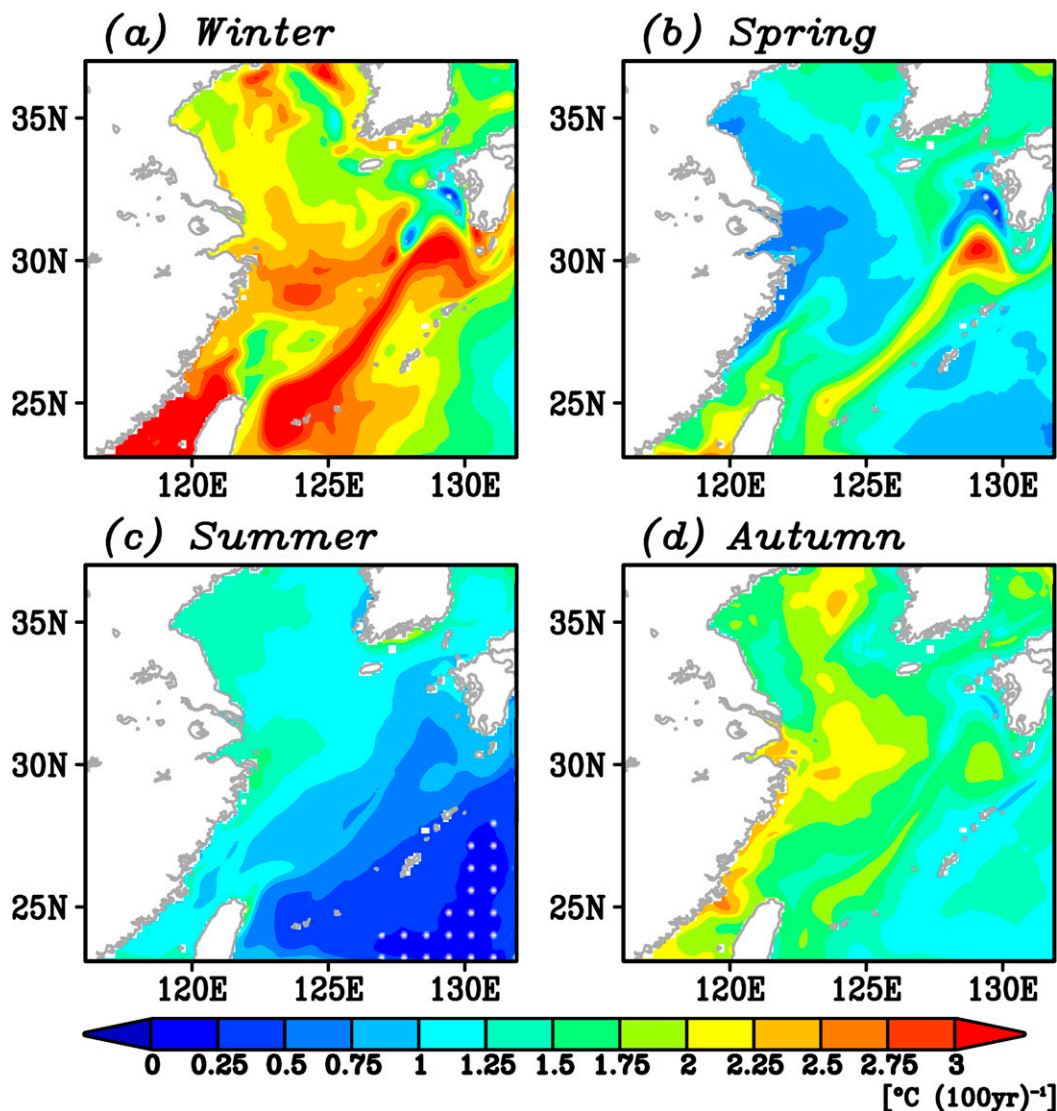


FIG. 6. Linear SST trend from the CTL run in (a) winter (January–March), (b) spring (April–June), (c) summer (July–September), and (d) autumn (October–December). The regions in which the trend is not statistically significant at a 95% confidence level are stippled.

heat advection averaged along the Kuroshio was large in winter and spring [$+3.3^{\circ}$ and $+3.9^{\circ}\text{Cyr}^{-1} (100\text{yr})^{-1}$, respectively]. The trend of the surface net heat flux along the Kuroshio was the largest in spring [$-4.3^{\circ}\text{Cyr}^{-1} (100\text{yr})^{-1}$], which was mainly explained by the latent heat flux trend along the Kuroshio axis (not shown). This large negative trend of the surface net heat flux in spring is consistent with the weak SST trend in summer along the Kuroshio (Figs. 6 and 7). On the other hand, the trends of the surface net heat flux averaged over the continental shelf were negative from winter to summer [from -1.0° to $-2.2^{\circ}\text{Cyr}^{-1} (100\text{yr})^{-1}$], roughly consistent with the weak SST trend over the continental shelf in spring and summer (Figs. 6 and 7). Interestingly, the trend of the surface net heat flux in autumn averaged over the continental shelf was positive [$+2.6^{\circ}\text{Cyr}^{-1} (100\text{yr})^{-1}$]. This implies that

although the annual mean surface heat flux acted to reduce the SST trend over the continental shelf, the surface heat flux in autumn induced the SST warming.

To further investigate the trend of the oceanic advection, the trend of the horizontal velocity averaged over 0–100 m was estimated (Fig. 10). Obviously, the Kuroshio is intensified in the surface layer, which is consistent with the increased temperature advection (Fig. 9c). The heat advection is frequently separated into the advection of mean temperature by the anomalous flow and the advection of anomalous temperature by the mean flow (e.g., Qiu 2000). Since there is the climatological temperature gradient along the Kuroshio maintained by the northward transport of the warm water and the gradual heat release from the ocean to the atmosphere (Fig. 2c), the increased temperature advection resulted from the advection

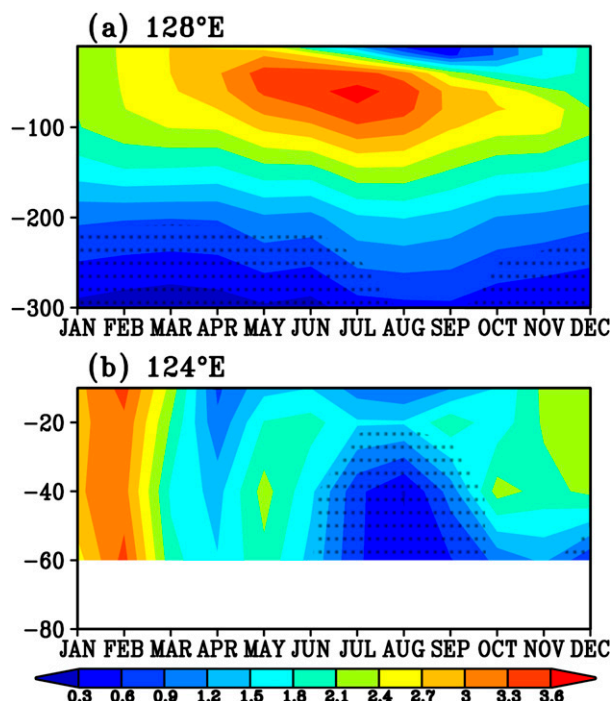


FIG. 7. Vertical section of the seasonal march of the temperature trend along 29°N (a) at 128°E and (b) at 124°E from 1901 to 2010 obtained from the CTL run. The units are $^{\circ}\text{C} (100\text{ yr})^{-1}$. The regions in which the trend is not statistically significant at a 95% confidence level are stippled.

of mean temperature by the anomalous flow. Because the anomalous poleward temperature gradient is not always negative along the Kuroshio path (Fig. 3c), the temperature advection of anomalous temperature by the mean flow was likely small. At the same time, the velocity trend over the continental shelf was not well organized. However, a closer inspection of the velocity change over the continental shelf indicates that the anomalous westward current around 29°N from the Kuroshio splits northward and southward along the coastline (Fig. 10b), which is likely consistent with the warming over the continental shelf. This velocity change over the continental shelf will be further investigated in the next subsection.

The vertical structure of the meridional velocity trend also revealed intensification of the Kuroshio (Fig. 11). The maximum of the trend was located in the uppermost layer and had an amplitude of $0.2\text{ m s}^{-1} (100\text{ yr})^{-1}$, which corresponded to approximately 30% of the climatological meridional velocity of the Kuroshio at this latitude ($\sim 0.7\text{ m s}^{-1}$). The increasing of the Kuroshio velocity extended to the deep layer and thus had an equivalent barotropic structure. This was different from the positive trend of the temperature, which was confined to the upper 400 m (Fig. 5). The difference can be explained by the horizontal temperature gradient in the deep layer. Because the horizontal temperature gradient along the Kuroshio in the deep layer was weakly negative poleward (not shown), the acceleration of the Kuroshio might also explain the negative temperature trend in this layer. In contrast to the Kuroshio

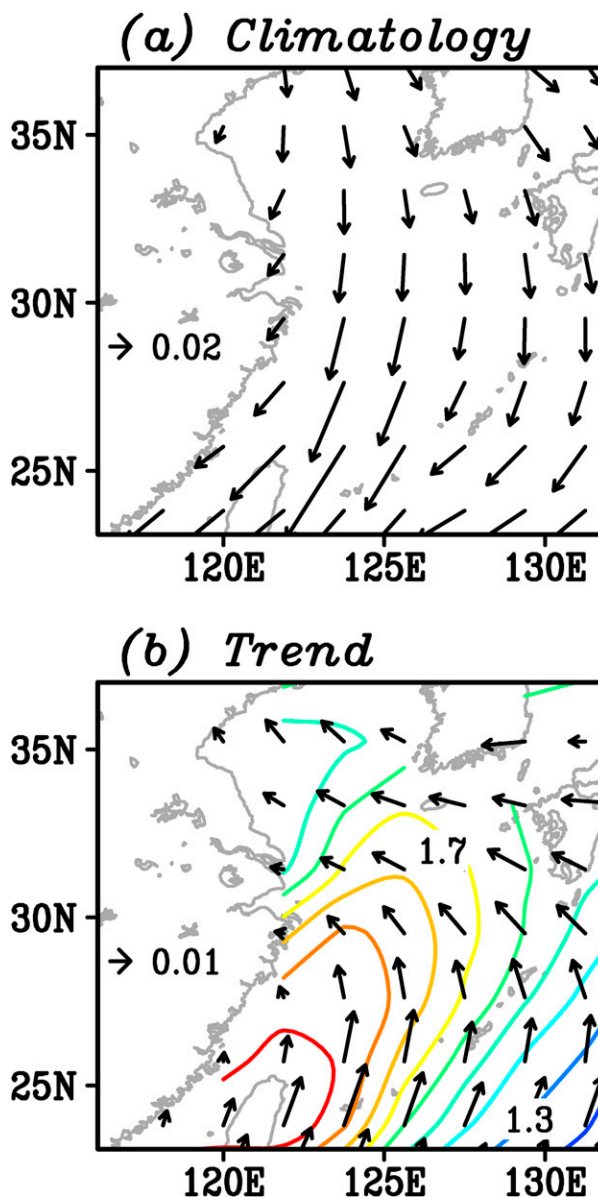


FIG. 8. (a) Climatology and (b) linear trend of the surface wind stress (vectors) of the 20CR data from 1901 to 2010. The units are N m^{-2} . The contours in (b) is the linear trend of 2-m air temperature of the 20CR data from 1901 to 2010. The contour interval is $0.1^{\circ}\text{C} (100\text{ yr})^{-1}$.

region, the meridional velocity trend over the continental shelf was small.

c. Sensitivity experiments

In the previous subsection, it was revealed from the CTL run that the temperature advection trend induced the rapid warming of the SST along the Kuroshio and along the China coast over the continental shelf (Fig. 9). We also demonstrated that the intensification of the Kuroshio caused the temperature advection trend (Fig. 11). However, the reason for the intensification

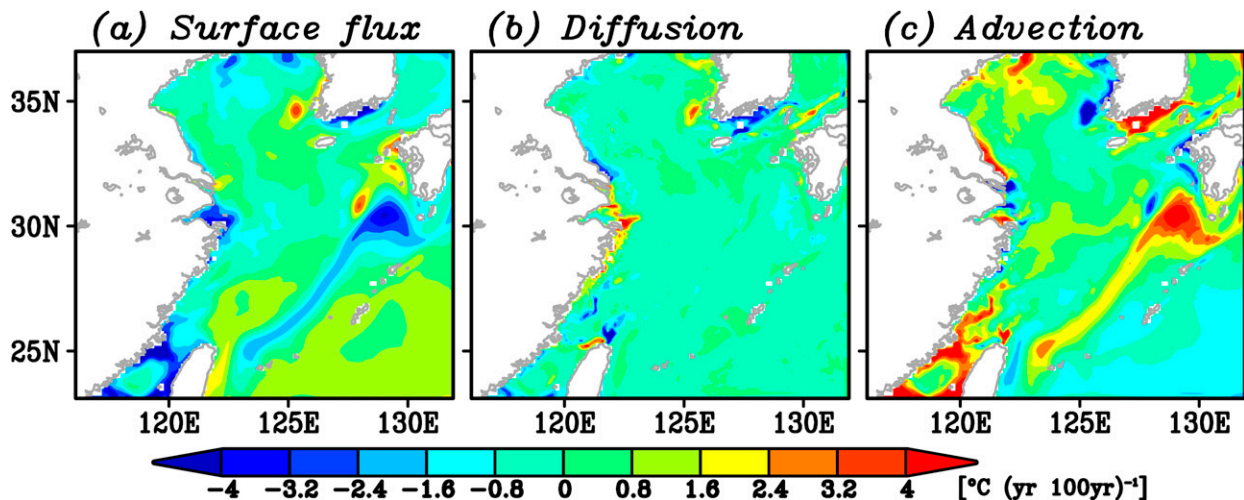


FIG. 9. Linear trend of (a) the surface heat flux term, (b) the diffusion term, and (c) the advection term of the temperature equation averaged over 0–100 m obtained from the CTL run from 1901 to 2010. A positive value indicates warming.

of the Kuroshio remains unclear. Previous studies had suggested that the fluctuations of the Kuroshio in the East China Sea and the associated ocean circulation changes over the continental shelf are induced not only by local atmospheric forcing over the East China Sea (e.g., Oey et al. 2010, 2013; Wu et al. 2014; Nakamura et al. 2015) but also by remote forcing from the North Pacific (e.g., Andres et al. 2009, 2011; Chen et al. 2019). Hence, it is important to clarify whether these advection trends are caused by the forcing over the East China Sea or by forcing outside the East China Sea. To clarify these points, we examined the results of the two sensitivity runs (the LOCAL and REMOTE runs). Note that because the response of the SST trends was not necessarily linear, the sum of the SST trends of the LOCAL and REMOTE runs was not generally equal to the SST trend of the CTL run.

Interestingly, the comparison of the SST trends of the LOCAL and REMOTE runs indicates that the mechanism of the SST trend is different between the areas along the Kuroshio and along the China coast over the continental shelf (Figs. 12a,b). The SST trend of the LOCAL run indicates that the rapid SST warming along the coast of China is caused by local forcing over the East China Sea (Fig. 12a), while the intrusion of the Kuroshio water onto the shelf in the REMOTE run also plays some roles in warming along the China coast (Fig. 12b). At the same time, the result of the REMOTE run indicates that the SST warming along the Kuroshio is induced by remote forcing from outside of the model domain (Fig. 12b). Except for along the Kuroshio, the SST trend in the East China Sea was relatively small in the REMOTE run. In contrast, the LOCAL run simulated a positive SST trend over the entire model domain except for along the Kuroshio. These results appear to be reasonable, as in general the warming of atmospheric temperature associated with global warming causes local SST warming.

First, we focused on the SST trend of the REMOTE run. In this run, the Kuroshio was also intensified in the East China Sea (not shown), and the amplitude of the Kuroshio intensification was comparable to that measured in the CTL run

(Fig. 10). The results of the REMOTE run imply that the intensification of the Kuroshio occurred not only in the East China Sea (Figs. 10 and 11) but also outside of the model domain. In line with this, the SODA reanalysis product, which is the lateral boundary conditions of the REMOTE run, suggested that the intensification of the Kuroshio extended southward to the east coast of Philippines (Fig. 13). These results indicate an increase in the inflow of the Kuroshio to the East China Sea, which is consistent with the SST warming along the Kuroshio measured in the REMOTE run (Fig. 12b). Note that the velocity trend along the Kuroshio in the East China Sea obtained in the CTL run (Fig. 10) was approximately 1.5 times larger than that obtained by the SODA reanalysis product (Fig. 13). In addition, the Kuroshio axis of the CTL run was shifted onshore (westward) compared with that of the SODA reanalysis product. These discrepancies were probably due to the difference in horizontal resolution between the models. In spite of these discrepancies, the location of the Kuroshio axis along the continental slope in the East China Sea is essentially not changed in the CTL run and the SODA reanalysis product (not shown).

It remains to be asked how the atmospheric forcing induces the intensification of the Kuroshio. To investigate the relation of the intensification of the Kuroshio to atmospheric change, we estimated the trend of the wind stress curl over the North Pacific, because the Kuroshio is the western boundary current of the subtropical gyre. The negative wind stress curl trend was found to be located over the North Pacific in a latitude range of 10°–20°N (Fig. 14), which is associated with weakening and southward shift of the trade wind. This wind stress curl trend indicates an increasing in the southward Sverdrup transport and is consistent with the intensification of the Kuroshio at the same latitude. It is also consistent with the fact that the intensification of the Kuroshio is not confined to the surface layer but extends to the deep layer (Fig. 11). It might be asked why the trend of the wind stress curl along the latitude of the East China Sea (~25°–30°N) was positive or close to zero. This is

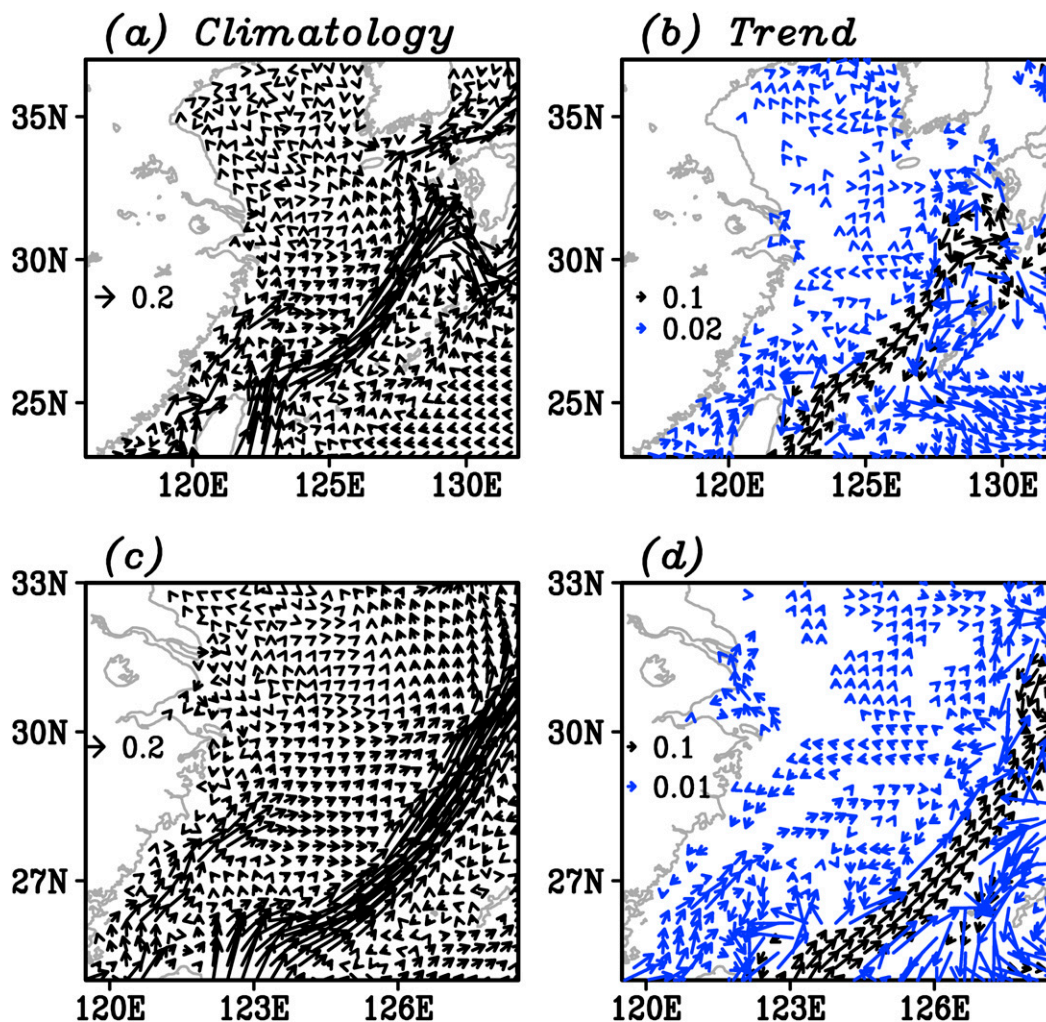


FIG. 10. (a) Climatology and (b) linear trend of the horizontal velocity averaged over 0–100 m from 1901 to 2010 obtained from the CTL run. In (b), the trends of the horizontal velocity that are larger and smaller than $0.1 \text{ m s}^{-1} (100 \text{ yr})^{-1}$ are shown as black and blue vectors, respectively. The arrow length scalings of the black and blue vectors are 0.1 and $0.02 \text{ m s}^{-1} (100 \text{ yr})^{-1}$, respectively. The vectors with both zonal and horizontal velocity trends that were not statistically significant at a 95% confidence level are not plotted. (c),(d) Enlarged views of (a) and (b), respectively. In (d), the arrow length scalings of the black and blue vectors are 0.1 and $0.01 \text{ m s}^{-1} (100 \text{ yr})^{-1}$, respectively.

probably because the Kuroshio transport in the East China Sea is not balanced in relation to the Sverdrup transport in the interior ocean due to the effect of the Ryukyu Islands (e.g., Kagimoto and Yamagata 1997). Akitomo et al. (1996) have also pointed out that temporal fluctuations of the Kuroshio transport in the East China Sea corresponded to those at the beginning of the Kuroshio south of 21°N , which is likely consistent with our results.

Next, the SST trend of the LOCAL run, especially the SST trend over the continental shelf, was investigated (Fig. 12a). As shown in Fig. 9c, this warming trend was induced by temperature advection change in the CTL run. This also holds true for the heat budget of the LOCAL run (not shown). Thus, we examined the horizontal velocity trend of the LOCAL run

(Fig. 15). Obviously, the intensification of the Kuroshio was quite weak in the LOCAL run. In contrast, a significant velocity trend was observed over the continental shelf (Fig. 15b). A closer inspection of the velocity trend along the China coast shows that the anomalous westward current around 29°N flowed over the continental shelf and was then split northward and southward along the coast. This anomalous westward current around 29°N corresponds to a weakening of the circulation over the continental shelf (see Fig. 10c), which might be consistent with the weakening of the northerly wind (Fig. 8). Yuan and Hsueh (2010) showed from numerical experiments that wintertime northerly wind over the East China Sea induced a meridional sea level tilt to the south and resulted in the eastward current over the continental shelf, likely consistent

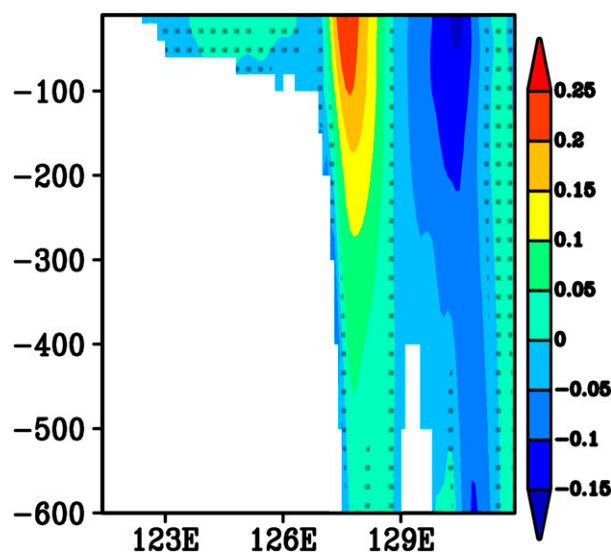


FIG. 11. As in Fig. 5, but for the meridional velocity along 29°N. The units are $\text{m s}^{-1} (100 \text{ yr})^{-1}$.

with our results. Since this anomalous westward current was able to transport warm water westward (see Fig. 2), its existence is consistent with the fast SST trend observed over the continental shelf. Note that this anomalous current over the continental shelf can be seen in the velocity trend of the CTL run (Fig. 10), although its structure is largely hidden by the large velocity trend associated with the intensification of the Kuroshio.

4. Summary and discussion

We examined the SST trend in the East China Sea from 1901 to 2010, mainly using a regional ocean model with an eddy-resolving horizontal resolution. It was demonstrated from the

two observational datasets and the CTL simulation that there were two broad peaks of the SST trend in the East China Sea (Fig. 3). These peaks reveal that the SST trend was large along the Kuroshio and along the China coast over the continental shelf, with the SST trends in these regions being about 2–3 times larger than the global mean SST trend (Fig. 4). Interestingly, the CTL run revealed that the SST trend along the Kuroshio was accompanied by subsurface maximums in the temperature trend at between 50 and 100 m (Fig. 5). Seasonally, the SST trends along the Kuroshio and the China coast have been the largest in winter (Fig. 6). The heat budget analysis of the CTL run revealed that increasing oceanic heat advection induced the upper layer temperature rise in both regions (Fig. 9). At the other time, the net surface heat flux, especially the latent heat release, was balanced in relation to the oceanic heat advection trend and acted to damp the upper-layer temperature trends. The importance of the advection in the SST trend along the Kuroshio found here is basically consistent with that determined by Zhang et al. (2010) and Cai et al. (2017), but the analysis period of the present study was nearly twice as long as those of the previous studies. The trend of the heat advection along the Kuroshio was caused by the acceleration of the Kuroshio (Fig. 10), extending to the deep layer (Fig. 11).

The sensitivity experiments revealed that the causes of the oceanic heat advection trend and thus the upper-layer temperature trend were different between the area along the Kuroshio and along the China coast (Fig. 12). The trend of the oceanic heat advection along the Kuroshio in the East China Sea was related to the intensification of the Kuroshio in an area outside of the model domain (Figs. 12b and 13). This intensification of the Kuroshio was likely caused by the increasing of the southward Sverdrup transport in response to the negative wind stress curl trends over the North Pacific (Fig. 14). In contrast, the enhanced SST warming along the China coast resulted from the ocean circulation change over the continental shelf caused by local atmospheric forcing change

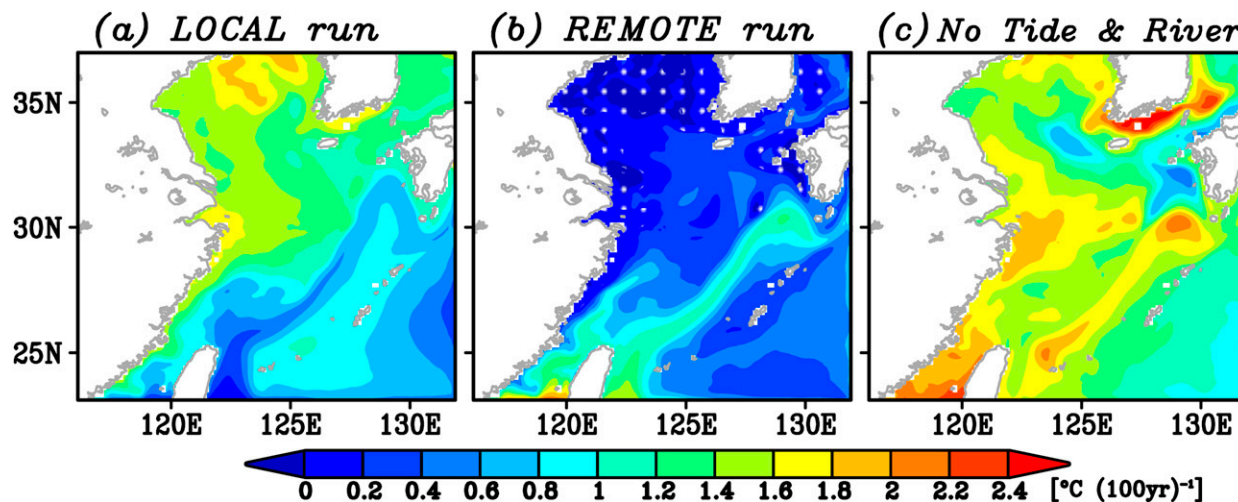


FIG. 12. As in Fig. 3c, but for (a) the LOCAL run, (b) the REMOTE run, and (c) the sensitivity run that does not include the tide and the Changjiang River discharge.

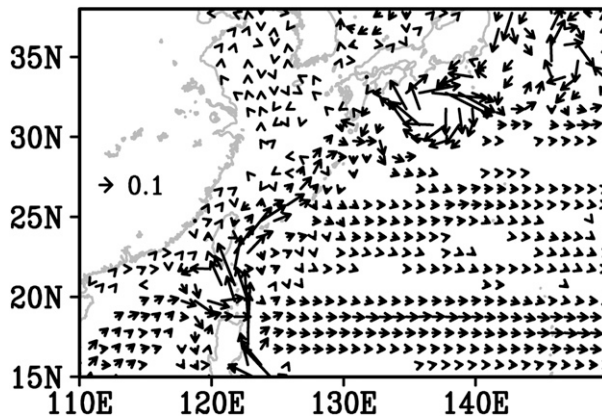


FIG. 13. As in Fig. 10b, but for the SODA reanalysis product. The units are $\text{m s}^{-1} (100 \text{ yr})^{-1}$. Only horizontal velocity trends above a 95% confidence level are plotted.

(Figs. 12a and 15). Note that the spatial pattern of the SST trend in the East China Sea in the CTL run is similar to that of the simulation without the tide and the Changjiang River discharge (Fig. 12c).

The present study examined the SST trend of the East China Sea during the twentieth century, but it is important to ask what the future changes in the SST will be. Manda et al. (2014) have demonstrated using regional atmospheric experiments that future warming of SST in the East China Sea could increase the frequency of torrential rainfall events over western Japan. Interestingly, Seo et al. (2014), who used the dynamical scaling with a regional ocean model in the western North Pacific, have reported on the weak SST trend from 2010 to 2100 along the Kuroshio in the East China Sea. Their results contrast with the results of the present study. We speculate that the difference is due to the difference in atmospheric circulation change, but we leave this problem for future study.

We also demonstrated that the enhanced SST warming in the East China Sea was caused by ocean circulation changes (Fig. 9). The resultant SST change then affected the atmospheric temperature. As mentioned in the introduction, the

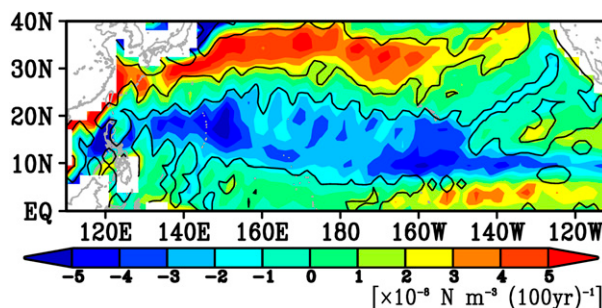


FIG. 14. Linear trend of the wind stress curl from 1901 to 2010 obtained from the 20CR data (shaded). The contour indicates the region in which the corresponding trend is statistically significant at a 95% confidence level.

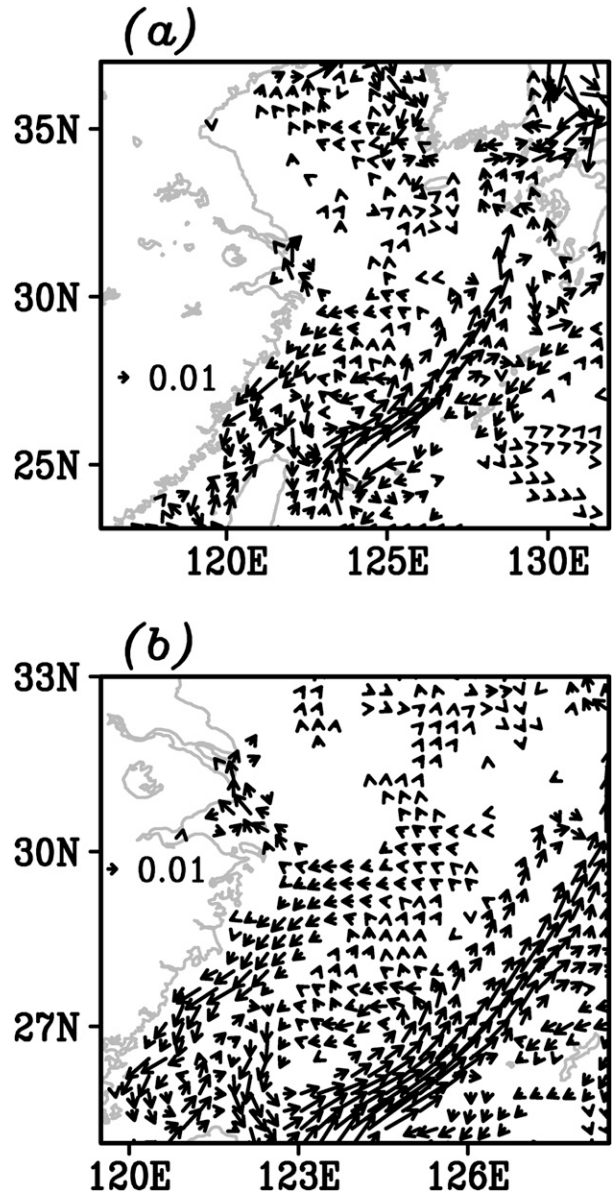


FIG. 15. As in Figs. 10b and 10d, but for the LOCAL run. The units are $\text{m s}^{-1} (100 \text{ yr})^{-1}$.

SST front between the Kuroshio and the continental shelf plays a key role in the influence of the ocean on the atmosphere. For example, Sasaki and Yamada (2018) have shown that the interannual variability of the SST front strength in June causes precipitation fluctuations over the East China Sea and southern Japan. However, determining whether or not the SST trend shown in the present study (Fig. 3) changes the SST front strength is not straightforward, as the large SST trends along the Kuroshio and the China coast are likely to strengthen and weaken the SST front, respectively. Hence, to determine the atmospheric response to the SST trend of the East China Sea, a future study using atmospheric model experiments would be necessary.

Acknowledgments. We thank Prof. S. Minobe and Prof. M. Inatsu for their valuable comments. We also thank three anonymous reviewers for their constructive comments on the manuscript. This research was supported by the Japan Society for the Promotion of Science (JSPS) KAKENHI Grants 19K03960 and 19H05704, which is funded by the Ministry of Education, Culture, Sports, Science, and Technology of Japan. The World Ocean Atlas 2009 dataset was downloaded from https://www.nodc.noaa.gov/OC5/WOA09/pr_woa09.html. The 20CR data were downloaded from https://psl.noaa.gov/data/gridded/data.20thC_ReanV2.html. The SODA reanalysis product was obtained from <http://abcmgr.tamu.edu/experiments.htm>. The three SST datasets (HadISST, Minobe/Maeda, and OISST) can be downloaded from <https://www.metoffice.gov.uk/hadobs/hadisst/data/download.html>, https://www.sci.hokudai.ac.jp/~minobe/data_by_minobe/sst_1dg_ICOADS/, and <https://www.ncdc.noaa.gov/oisst>, respectively. The river discharge dataset was downloaded from <https://rda.ucar.edu/datasets/ds551.0/>.

REFERENCES

- Akitomo, K., M. Ooi, T. Awaji, and K. Kutsuwada, 1996: Interannual variability of the Kuroshio transport in response to the wind stress field over the North Pacific: Its relation to the path variation south of Japan. *J. Geophys. Res.*, **101**, 14 057–14 071, <https://doi.org/10.1029/96JC01000>.
- Andres, M., J. H. Park, M. Wimbush, X. H. Zhu, H. Nakamura, K. Kim, and K. I. Chang, 2009: Manifestation of the Pacific decadal oscillation in the Kuroshio. *Geophys. Res. Lett.*, **36**, L16602, <https://doi.org/10.1029/2009GL039216>.
- , Y.-O. Kwon, and J. Yang, 2011: Observations of the Kuroshio's barotropic and baroclinic responses to basin-wide wind forcing. *J. Geophys. Res.*, **116**, C04011, <https://doi.org/10.1029/2010JC006863>.
- Antonov, J. I., and Coauthors, 2010: *Salinity*. Vol. 2, *World Ocean Atlas 2009*, NOAA Atlas NESDIS 69, 184 pp.
- Bao, B., and G. Ren, 2014: Climatological characteristics and long-term change of SST over the marginal seas of China. *Cont. Shelf Res.*, **77**, 96–106, <https://doi.org/10.1016/j.csr.2014.01.013>.
- Belkin, I. M., 2009: Rapid warming of large marine ecosystems. *Prog. Oceanogr.*, **81**, 207–213, <https://doi.org/10.1016/j.pocean.2009.04.011>.
- Cai, R., H. Tan, and H. Kontoyiannis, 2017: Robust surface warming in offshore China seas and its relationship to the East Asian monsoon wind field and ocean forcing on interdecadal time scales. *J. Climate*, **30**, 8987–9005, <https://doi.org/10.1175/JCLI-D-16-0016.1>.
- Chen, C., G. Wang, S. Xie, and W. Liu, 2019: Why does global warming weaken the Gulf Stream but intensify the Kuroshio? *J. Climate*, **32**, 7437–7451, <https://doi.org/10.1175/JCLI-D-18-0895.1>.
- Compo, G. P., and Coauthors, 2011: The Twentieth Century Reanalysis Project. *Quart. J. Roy. Meteor. Soc.*, **137**, 1–28, <https://doi.org/10.1002/qj.776>.
- Dai, A., and K. E. Trenberth, 2002: Estimates of freshwater discharge from continents: Latitudinal and seasonal variations. *J. Hydrometeorol.*, **3**, 660–687, [https://doi.org/10.1175/1525-7541\(2002\)003<0660:EOFDFO>2.0.CO;2](https://doi.org/10.1175/1525-7541(2002)003<0660:EOFDFO>2.0.CO;2).
- Egbert, G. D., and S. Y. Erofeeva, 2002: Efficient inverse modeling of barotropic ocean tides. *J. Atmos. Oceanic Technol.*, **19**, 183–204, [https://doi.org/10.1175/1520-0426\(2002\)019<0183:EIMOBO>2.0.CO;2](https://doi.org/10.1175/1520-0426(2002)019<0183:EIMOBO>2.0.CO;2).
- Fairall, C. W., E. F. Bradley, D. P. Rogers, J. B. Edson, and G. S. Young, 1996: Bulk parameterization of air–sea fluxes for Tropical Ocean–Global Atmosphere Coupled Ocean–Atmosphere Response Experiment. *J. Geophys. Res.*, **101**, 3747–3764, <https://doi.org/10.1029/95JC03205>.
- Giese, B. S., and S. Ray, 2011: El Niño variability in simple ocean data assimilation (SODA), 1871–2008. *J. Geophys. Res.*, **116**, C02024, <https://doi.org/10.1029/2010JC006695>.
- Guo, X., H. Hukuda, Y. Miyazawa, and T. Yamagata, 2003: A triply nested ocean model for simulating the Kuroshio—Roles of horizontal resolution on JEBAR. *J. Phys. Oceanogr.*, **33**, 146–169, [https://doi.org/10.1175/1520-0485\(2003\)033<0146:ATNOMF>2.0.CO;2](https://doi.org/10.1175/1520-0485(2003)033<0146:ATNOMF>2.0.CO;2).
- Haidvogel, D. B., H. G. Arango, K. Hedstrom, A. Beckmann, P. Malanotte-Rizzoli, and A. F. Schepetkin, 2000: Model evaluation experiments in the North Atlantic basin: Simulations in nonlinear terrain-following coordinates. *Dyn. Atmos. Oceans*, **32**, 239–281, [https://doi.org/10.1016/S0377-0265\(00\)00049-X](https://doi.org/10.1016/S0377-0265(00)00049-X).
- Kagimoto, T., and T. Yamagata, 1997: Seasonal transport variations of the Kuroshio: An OGCM simulation. *J. Phys. Oceanogr.*, **27**, 403–418, [https://doi.org/10.1175/1520-0485\(1997\)027<0403:STVOTK>2.0.CO;2](https://doi.org/10.1175/1520-0485(1997)027<0403:STVOTK>2.0.CO;2).
- Kako, S., T. Nakagawa, K. Takayama, N. Hirose, and A. Isobe, 2016: Impact of Changjiang River discharge on sea surface temperature in the East China Sea. *J. Phys. Oceanogr.*, **46**, 1735–1750, <https://doi.org/10.1175/JPO-D-15-0167.1>.
- Kaplan, D., and L. Glass, 1995: *Understanding Nonlinear Dynamics*. Springer-Verlag, 420 pp.
- Kelly, K. A., R. J. Small, R. M. Samelson, B. Qiu, T. M. Joyce, Y.-O. Kwon, and M. F. Cronin, 2010: Western boundary currents and frontal air–sea interaction: Gulf Stream and Kuroshio Extension. *J. Climate*, **23**, 5644–5667, <https://doi.org/10.1175/2010JCLI3346.1>.
- Kida, S., and Coauthors, 2015: Oceanic fronts and jets around Japan: A review. *J. Oceanogr.*, **71**, 469–497, <https://doi.org/10.1007/s10872-015-0283-7>.
- Levitus, S., J. I. Antonov, T. P. Boyer, R. A. Locarnini, H. E. Garcia, and A. V. Mishonov, 2009: Global ocean heat content 1955–2008 in light of recently revealed instrumentation problems. *Geophys. Res. Lett.*, **36**, L07608, <https://doi.org/10.1029/2008GL037155>.
- Lin, L., D. Liu, X. Guo, C. Luo, and Y. Cheng, 2020: Tidal effect on water export rate in the eastern shelf seas of China. *J. Geophys. Res. Oceans*, **125**, e2019JC015863, <https://doi.org/10.1029/2019JC015863>.
- Locarnini, R. A., and Coauthors, 2010: *Temperature*. Vol. 1, *World Ocean Atlas 2009*, NOAA Atlas NESDIS 68, 184 pp.
- Manda, A., and Coauthors, 2014: Impacts of a warming marginal sea on torrential rainfall organized under the Asian summer monsoon. *Sci. Rep.*, **4**, 5741, <https://doi.org/10.1038/srep05741>.
- Minobe, S., and A. Maeda, 2005: A 1° monthly gridded sea-surface temperature dataset compiled from ICOADS from 1850 to 2002 and Northern Hemisphere frontal variability. *Int. J. Climatol.*, **25**, 881–894, <https://doi.org/10.1002/joc.1170>.
- Miyama, T., M. Nonaka, H. Nakamura, and A. Kuwano-Yoshida, 2012: A striking early-summer event of a convective rainband persistent along the warm Kuroshio in the East China Sea. *Tellus*, **64A**, 18962, <https://doi.org/10.3402/tellusa.v64i0.18962>.
- Na, H., M. Wimbush, J.-H. Park, H. Nakamura, and A. Nishina, 2014: Observations of flow variability through the Kerama Gap between the East China Sea and the northwestern Pacific. *J. Geophys. Res. Oceans*, **119**, 689–703, <https://doi.org/10.1002/2013JC008899>.
- Nakamura, H., R. Hiranaka, D. Ambe, and T. Saito, 2015: Local wind effect on the Kuroshio path state off the southeastern

- coast of Kyushu. *J. Oceanogr.*, **71**, 575–596, <https://doi.org/10.1007/s10872-015-0309-1>.
- Oey, L. Y., Y. C. Hsin, and C. R. Wu, 2010: Why does the Kuroshio northeast of Taiwan shift shelfward in winter? *Ocean Dyn.*, **60**, 413–426, <https://doi.org/10.1007/s10236-009-0259-5>.
- , M. C. Chang, Y. L. Chang, Y. C. Lin, and F. H. Xu, 2013: Decadal warming of coastal China seas and coupling with winter monsoon and currents. *Geophys. Res. Lett.*, **40**, 6288–6292, <https://doi.org/10.1002/2013GL058202>.
- Qiu, B., 2000: Interannual variability of the Kuroshio Extension and its impact on the wintertime SST field. *J. Phys. Oceanogr.*, **30**, 1486–1502, [https://doi.org/10.1175/1520-0485\(2000\)030<1486:IVOTKE>2.0.CO;2](https://doi.org/10.1175/1520-0485(2000)030<1486:IVOTKE>2.0.CO;2).
- Rayner, N. A., and Coauthors, 2003: Global analyses of sea surface temperature, sea ice, and night marine air temperature since the late nineteenth century. *J. Geophys. Res.*, **108**, 4407, <https://doi.org/10.1029/2002JD002670>.
- Reynolds, R. W., T. M. Smith, C. Liu, D. B. Chelton, K. S. Casey, and M. G. Schlax, 2007: Daily high-resolution-blended analyses for sea surface temperature. *J. Climate*, **20**, 5473–5496, <https://doi.org/10.1175/2007JCLI1824.1>.
- Rhein, M., and Coauthors, 2013: Observations: Ocean. *Climate Change 2013: The Physical Science Basis*, T. F. Stocker et al., Eds., Cambridge University Press, 255–315.
- Santer, B. D., and Coauthors, 2000: Statistical significance of trends and trend differences in layer-average atmospheric temperature time series. *J. Geophys. Res.*, **105**, 7337–7356, <https://doi.org/10.1029/1999JD901105>.
- Sasaki, Y. N., and N. Schneider, 2011: Interannual to decadal Gulf Stream variability in an eddy-resolving ocean model. *Ocean Modell.*, **39**, 209–219, <https://doi.org/10.1016/j.ocemod.2011.04.004>.
- , and Y. Yamada, 2018: Atmospheric response to interannual variability of sea surface temperature front in the East China Sea in early summer. *Climate Dyn.*, **51**, 2509–2522, <https://doi.org/10.1007/s00382-017-4025-y>.
- , S. Minobe, T. Asai, and M. Inatsu, 2012: Influence of the Kuroshio in the East China Sea on the early summer (baisu) rain. *J. Climate*, **25**, 6627–6645, <https://doi.org/10.1175/JCLI-D-11-00727.1>.
- Seo, G.-H., Y.-K. Cho, B.-J. Choi, K.-Y. Kim, B. Kim, and Y. Tak, 2014: Climate change projection in the northwest Pacific marginal seas through dynamic downscaling. *J. Geophys. Res. Oceans*, **119**, 3497–3516, <https://doi.org/10.1002/2013JC009646>.
- Shchepetkin, A. F., and J. C. McWilliams, 2005: The Regional Oceanic Modeling System (ROMS): A split-explicit, free-surface, topography-following-coordinate oceanic model. *Ocean Modell.*, **9**, 347–404, <https://doi.org/10.1016/j.ocemod.2004.08.002>.
- Small, R. J., and Coauthors, 2008: Air–sea interaction over ocean fronts and eddies. *Dyn. Atmos. Oceans*, **45**, 274–319, <https://doi.org/10.1016/j.dynatmoce.2008.01.001>.
- Tang, X., F. Wang, Y. Chen, and M. Li, 2009: Warming trend in northern East China Sea in recent four decades. *Chin. J. Oceanol. Limnol.*, **27**, 185–191, <https://doi.org/10.1007/s00343-009-9238-4>.
- Trenberth, K. E., and Coauthors, 2007: Observations: Surface and atmospheric climate change. *Climate Change 2007: The Physical Science Basis*, S. Solomon et al., Eds., Cambridge University Press, 235–336.
- Wilkin, J. L., 2006: The summertime heat budget and circulation of southeast New England shelf waters. *J. Phys. Oceanogr.*, **36**, 1997–2011, <https://doi.org/10.1175/JPO2968.1>.
- Wu, C. R., Y. C. Hsin, T. L. Chiang, Y. F. Lin, and I. F. Tsui, 2014: Seasonal and interannual changes of the Kuroshio intrusion onto the East China Sea shelf. *J. Geophys. Res. Oceans*, **119**, 5039–5051, <https://doi.org/10.1002/2013JC009748>.
- Wu, L. X., and Coauthors, 2012: Enhanced warming over the global subtropical western boundary currents. *Nat. Climate Change*, **2**, 161–166, <https://doi.org/10.1038/nclimate1353>.
- Xie, S.-P., J. Hafner, Y. Tanimoto, W. T. Liu, H. Tokinaga, and H. Xu, 2002: Bathymetric effect on the winter sea surface temperature and climate of the Yellow and East China Seas. *Geophys. Res. Lett.*, **29**, 2228, <https://doi.org/10.1029/2002GL015884>.
- , C. Deser, G. A. Vecchi, J. Ma, H. Teng, and A. T. Wittenberg, 2010: Global warming pattern formation: Sea surface temperature and rainfall. *J. Climate*, **23**, 966–986, <https://doi.org/10.1175/2009JCLI3329.1>.
- Xu, H., M. Xu, S.-P. Xie, and Y. Wang, 2011: Deep atmospheric response to the spring Kuroshio over the East China Sea. *J. Climate*, **24**, 4959–4972, <https://doi.org/10.1175/JCLI-D-10-05034.1>.
- Yang, D. Z., B. S. Yin, Z. L. Liu, and X. R. Feng, 2011: Numerical study of the ocean circulation on the East China Sea shelf and a Kuroshio bottom branch northeast of Taiwan in summer. *J. Geophys. Res.*, **116**, C05015, <https://doi.org/10.1029/2010JC006777>.
- Yang, H., G. Lohmann, W. Wei, M. Dima, M. Ionita, and J. Liu, 2016: Intensification and poleward shift of subtropical western boundary currents in a warming climate. *J. Geophys. Res. Oceans*, **121**, 4928–4945, <https://doi.org/10.1002/2015JC011513>.
- Yeh, S.-W., and C.-H. Kim, 2010: Recent warming in the Yellow/East China Sea during winter and the associated atmospheric circulation. *Cont. Shelf Res.*, **30**, 1428–1434, <https://doi.org/10.1016/j.csr.2010.05.002>.
- Yuan, D., and Y. Hsueh, 2010: Dynamics of the cross-shelf circulation in the Yellow and East China Seas in winter. *Deep-Sea Res. II*, **57**, 1745–1761, <https://doi.org/10.1016/j.dsr2.2010.04.002>.
- Zhang, L., L. Wu, X. Lin, and D. Wu, 2010: Modes and mechanisms of sea surface temperature low-frequency variations over the coastal China seas. *J. Geophys. Res.*, **115**, C08031, <https://doi.org/10.1029/2009JC006025>.